Published in final edited form as:
DNA Repair (Amst). 2012 September 1; 11(9): 753–765. doi:10.1016/j.dnarep.2012.06.008.

Saccharomyces cerevisiae Apn1 Mutation Affecting Stable Protein Expression Mimics Catalytic Activity Impairment: Implications for Assessing DNA Repair Capacity in Humans

Lydia P. Morris[a,b], **Natalya Degtyareva**[b], **Clayton Sheppard**[c], **Lanier Heyburn**[b], **Andrei A. Ivanov**[d], **Yoke Wah Kow**[c], and **Paul W. Doetsch**[b,c,e,f,g]

[a]Program in Genetics and Molecular Biology, Graduate Division of Biological and Biomedical Sciences, James T. Laney School of Graduate Studies, Emory University

[b]Department of Biochemistry, Emory University School of Medicine, Atlanta, GA 30322, USA

[c]Department of Radiation Oncology, Emory University School of Medicine, Atlanta, GA 30322, USA

[d]Emory Chemical Biology Discovery Center, Emory University School of Medicine, Atlanta, GA 30322, USA

[e]Department of Hematology and Medical Oncology, Emory University School of Medicine, Atlanta, GA 30322, USA

[f]Winship Cancer Institute, Emory University School of Medicine, Atlanta, GA 30322, USA

Abstract

Apurinic/apyrimidinic (AP) endonucleases play a major role in the repair of AP sites, oxidative damage and alkylation damage in DNA. We employed *Saccharomyces cerevisiae* in an unbiased forward genetic screen to identify amino acid substitutions in the major yeast AP endonuclease, Apn1, that impair cellular DNA repair capacity by conferring sensitivity to the DNA alkylating agent methyl methanesulfonate. We report here the identification and characterization of the Apn1 V156E amino acid substitution mutant through biochemical and functional analysis. We found that steady-state levels of Apn1 V156E were substantially decreased compared to wild type protein, and that this decrease was due to more rapid degradation of mutant protein compared to wild type. Based on homology to *E. coli* endonuclease IV and computational modeling, we predicted that V156E impairs catalytic ability. However, overexpression of mutant protein restored DNA repair activity *in vitro* and *in vivo*. Thus, the V156E substitution decreases DNA repair capacity by an unanticipated mechanism via increased degradation of mutant protein, leading to substantially reduced cellular levels. Our study provides evidence that the V156 residue plays a critical role in Apn1 structural integrity, but is not involved in catalytic activity. These results have important implications for elucidating structure-function relationships for the endonuclease IV family of proteins, and for employing simple eukaryotic model systems to

[g]Corresponding author: Phone: 404-727-0409, Fax: 404-727-3231, medpwd@emory.edu.

Conflict of interest statement
The authors declare that there are no conflicts of interest.

understand how structural defects in the major human AP endonuclease APE1 may contribute to disease etiology.

Keywords

Structure-function relationship; AP endonuclease; Single nucleotide polymorphism; Apn1; Methyl methanesulfonate

1. Introduction

The base excision repair (BER) pathway is essential for protection against the continuous oxidation, alkylation and hydrolysis of DNA due to normal cellular metabolism and environmental DNA damaging agents. Such genotoxic exposures result in the formation of base lesions, apurinic/apyrimidinic (AP) sites and DNA strand breaks. The production of AP sites, which are potentially cytotoxic [1, 2] and mutagenic [1, 3], occurs frequently as bases are spontaneously lost from the DNA backbone at an estimated rate of 10,000 per cell per day in mammals [4, 5]. AP sites are also generated as byproducts of the BER process through enzymatic removal of damaged bases by lesion-specific glycosylases that recognize and cleave base lesions from the DNA backbone [6, 7]. AP endonucleases recognize and nick the DNA backbone at AP sites followed by repair synthesis by DNA polymerase and sealing of the nicked DNA strand by ligase. AP endonucleases also function as 3′ diesterases to process 3′ blocked termini of single strand breaks produced as a result of oxidative damage [8]. Thus, AP endonucleases are central to the repair of a large subset of DNA damage within the cell via their ability to process major types of DNA damage that arise directly or that are produced as DNA repair intermediates.

Point mutations and SNPs in the human AP endonuclease APE1 that cause non-synonymous amino acid substitutions have been a focus of many epidemiological disease association studies [9, 10], and combined with computational modeling and experimental validation [11, 12], have provided clues regarding their roles in disease. For example, a previous study reporting *in vitro* biochemical characterization of APE1 variants identified from amyotrophic lateral sclerosis patients and several variants reported in the NCBI database of SNPs, confirmed that some of the APE1 variants with predicted catalytic defects indeed cause decreased catalytic activity while other variants exhibited normal activity [10]. This suggests that if such “neutral” substitutions are associated with disease risk, the defects may influence aspects of APE1 biology that were not measured, such as steady-state expression level, *in vivo* repair capacity or interactions with other BER proteins. Studies in higher eukaryotes are complicated by factors such as inter-individual genetic variation and molecular differences in repair capacity from one cell type to another, which present major challenges to identifying the molecular basis of AP endonuclease dysfunction in disease [10].

In order to explore how structural defects that compromise a critical, central step in the BER pathway manifest themselves in eukaryotic cells, we have investigated Apn1, the major AP endonuclease in *Saccharomyces cerevisiae* [13]. Apn1 is a functional homolog of mammalian APE1 as cross species complementation studies have shown that Apn1 can functionally complement the absence of APE1 DNA repair activity in human and other mammalian cells [14–16]. A major advantage of utilizing yeast for our studies is that Apn1 has no known DNA repair-independent activities, unlike human APE1, which does have other activities [17 18, 19] including functioning as a transcriptional co-activator of a number of genes. Studying yeast Apn1 allows for directly examining the cellular effects of

AP endonuclease catalytic deficiency, whereas genetic manipulation of the human APE1 could also influence its non-DNA repair activities.

Apn1 is a member of the endonuclease IV (endo IV) family of AP endonucleases. Previous biochemical and structural studies of *E. coli* endo IV have defined the molecular mechanisms by which DNA binding and phosphodiester bond incision are achieved for this family of enzymes [20–23]. This information provides a framework for exploring the functional consequences of particular changes in endonuclease structure.

To identify functionally relevant changes in Apn1 structure, we performed an unbiased random mutagenesis screen for mutants displaying sensitivity to the DNA alkylating agent methyl methanesulfonate. We report here the investigation of Apn1 structure-function relationship through characterization of a recessive mutation in the endogenous *APN1* locus that affects cellular repair capacity by an unanticipated mechanism. The V156E substitution leads to production of a full-length mutant protein with intact catalytic function even though predictions based on homology modeling suggested the possibility of catalytic domain dysfunction. Instead, we find that accelerated degradation of V156E leads to decreased cellular protein levels and defects in DNA repair. This unexpected mechanism of impaired DNA repair capacity suggests a role for V156 in the maintenance Apn1 structural integrity. Our findings have important implications for elucidating the functional consequences of SNPs mapping outside the known APE1 functional domains predicted to impact DNA repair, and illustrate the utility for employing simple model systems for such studies.

2. Materials and methods

2.1. Yeast cell culture conditions and transformation

Standard yeast media and cell culture conditions were used as previously described [24, 25]. Methyl methanesulfonate (MMS) (Sigma) was added to YPD medium at 0.08% after autoclaving and cooling. The lithium acetate method for yeast cell transformation was employed as previously described [25]. The sequences of primers and oligonucleotides used in this study are available upon request.

2.2. Plasmid construction

Details for plasmids used in this study are listed in Table S1.

Plasmid pD428, a CEN plasmid with wild type *APN1* inserted at the multiple cloning site (MCS) of pRS316 [26], was constructed by gap-repair cloning [27]. Briefly, PCR products with homology upstream of the SacI restriction site at the 5′ end and homology downstream of the Kpn1 restriction site at the 3′ end (with respect to the pRS316 MCS) were amplified using genomic DNA from strain DSC320 (Table 1). The resulting *APN1*-SacI/Kpn1I fragment was co-transformed with linearized pRS316 (digested with SacI and KpnI). Plasmids were then recovered, propagated in *E.coli*, and verified via restriction analysis and sequencing.

Plasmids pD433, pD434 and pD435 containing mutant versions of *APN1* (*apn1-V156E*, *apn1-E207V*, *apn1-V156E, E207V,* respectively) were constructed via site-directed mutagenesis of plasmid pD428 using the QuickChange site-directed mutagenesis kit from Stratagene.

2.3. Genetic manipulations

All *S. cerevisiae* strains used in this study are listed in Table 1. The parental strain DSC320 is a haploid spore of the diploid strain hDNP16 [28], and strains DSC386, DSC393 and DSC378 are haploid spores of the diploid strain hDNP19 [28]. Strain DSC320 does not

contain mutations in BER genes *APN1, NTG1* or *NTG2*. Strain DSC386 is *APN1*-deficient (*apn1Δ*). Strain DSC393 is *NTG1*- and *NTG2*-deficient (*ntg1Δ ntg2Δ*). Strain DSC378 is deficient in *APN1, NTG1* and *NTG2* (*apn1Δ ntg1Δ ntg2Δ*).

The *delitto perfetto* method [29] was used to target random PCR-generated mutations to the chromosomal *APN1* locus in a random mutagenesis screen (described in this section below), and to create site-directed mutations in the *APN1* locus (described in this section below). *I-SceI* CORE insertion strains were constructed using plasmid pGSKU as a PCR template to amplify an *apn1::KlURA3*-KanMX4-I-SceI fragment for transformation. The resulting *apn1::I-SceI* CORE insertion strains are DSC501 and DSC502 (Table 1).

For the random mutagenesis screen, plasmid pD428 was used as a template to generate a library of mutant *apn1* PCR fragments via amplification of the *APN1* coding sequence with a relaxed-fidelity PCR protocol described previously [30]. The library of mutant *apn1* fragments was introduced into the chromosomal *APN1* locus of CORE insertion strains DSC501 or DSC502 via *delitto perfetto*. Mutants were selected based on sensitivity to MMS by replica plating of transformants to medium containing 0.08% MMS. Only G418-sensitive and Ura$^-$ clones were considered for further analysis. Once mutant clones were purified, sensitivity to MMS was re-checked via serial dilution assay (described in section 2.4). Strain YDM10 was selected as an MMS-sensitive transformant in the genetic screen as described below.

Strains DSC517, DSC518, DSC519 and DSC520 were constructed in order to introduce the mutant alleles *apn1-V156E, E207V* and *apn1-V156E* and *apn1-E207V*, respectively, into non-mutagenized backgrounds. This was done by performing site-directed mutagenesis via *delitto perfetto* of CORE insertion strains DSC501 and DSC502. CORE deletion was performed by transforming the CORE insertion strains with PCR-generated fragments using as templates plasmids pD433, pD434 and PD435 that carry the different mutant versions of *APN1* (section 2.2 and Table S1).

Wild type and mutant strains expressing C-terminal Tandem Affinity Purification (TAP)-tagged Apn1 variants were constructed as follows: an *APN1*-TAP PCR fragment was generated via PCR amplification using the template plasmid pBS1479 [31]. The PCR product was used to transform strains DSC0320, DSC517, DSC519 and DSC520 to create DSC503, DSC521, DSC522, and DSC523 C-terminal TAP-tagged strains, respectively.

Wild type and mutant strains containing the *GAL1* promoter integrated directly upstream of the chromosomal *APN1* coding sequence were constructed as follows: a P_{GAL1}-*APN1* DNA fragment was amplified by PCR using pBS1761 [31] as a template. Strains DSC320, DSC522 and DSC523 were transformed with the resulting PCR fragment to create DSC504, DSC525, DSC526, respectively. Integration of the *GAL1* promoter at the *APN1* locus was confirmed by PCR. Wild type and mutant *APN1* strains expressing N-terminal TAP tagged versions of Apn1 under the control of the *GAL1* promoter at the chromosomal *APN1* locus were constructed as follows: a P_{GAL1}-TAP-*APN1* DNA fragment was amplified by PCR using pBS1761 as a template. Strains DSC320 and DSC519 were transformed with the resulting PCR fragment to create DSC436 and DSC545, respectively. Integration of the P_{GAL1}-TAP construct at the *APN1* locus was confirmed by PCR.

2.4. Analysis of MMS sensitivity

To test sensitivity of yeast cells to MMS, approximately equal numbers of cells were picked from streaks on YPD plates, and 5-fold serial dilutions of cells were plated onto media containing only YPD or YPD with 0.08% MMS. For P_{GAL1}-*APN1* overexpression experiments, cells were plated onto YPD as described above and media containing only YP-

galactose or YP-galactose with 0.08% MMS. Plates were incubated for 2 days at 30°C and then analyzed for sensitivity.

2.5. Homology modeling

The amino acid residue sequences of Apn1 and endo IV orthologs from bacterial, fungal, and metazoan organisms were downloaded from the UniProt database [32]. A sequence alignment was then performed with the ClusterX program using the BLOSUM protein weight matrix [33]. One of the closest homologs of Apn1 (41% amino acid identity) with an available protein crystal structure is *E.coli* endo IV. The structure of endo IV (PDB ID: 1qum) was used as the main template to build a homology model of the central region of Apn1. Because the C-terminus of endo IV is 67 amino acid residues shorter than Apn1, it cannot be used as a template to model the C-terminus of Apn1. A BLAST search was performed for the C-terminal part of Apn1 and sequence fragments from three proteins: foldase protein PrsA (PDB ID: 2JZV), fructose-1, 6-bisphosphatase (PDB ID: 2JJK), and hexokinase-1 (PDB ID: 1BG3). Although Apn1, PrsA, F16BP and hexokinase are not functionally related, these other proteins share significant sequence similarity with the C-terminal domain of Apn1, and can thus be used as acceptable templates for homology modeling. The sequence fragments from these three proteins were highly identical with the sequence fragments of the C-terminal domain of Apn1. The sequences of these three proteins were aligned with the Apn1 sequence, and their structures were used as templates. The homology model of wild type Apn1 was generated with the Modeller v9.7 program [34]. The default values were used for all parameters, except the following: the number of models to generate = 25, library_schedule = 10000, library_schedule = autosched.slow, md_level = refine.very_slow. Ten additional models were generated for each of the loop regions with the md_level parameter set to refine.very_slow. The most accurate model was selected based on the calculated values of DOPE, GA341, and normalized DOPE scoring functions. The Apn1 model was further refined with the Protein Preparation Wizard implemented in the Schrödinger Suite [35–37], and subjected to 1000 iterations of Polak-Riber Conjugate Gradient minimization in the MMFFs force field with the Schrödinger MacroModel program [35–37].

Homology models of Apn1 protein variants were derived from the refined wild type Apn1 model with the Maestro program of the Schrödinger Suite [38], and optimized by energy minimization as described above. Models of Apn1 variants were subjected to Monte Carlo Conformational Search analysis performed for the mutated residue and all residues within 5Å. The residues within an additional 2Å were used as a constrained shell. The Mixed torsional/Low-mode sampling method was utilized, the maximum number of steps was set to 500, and 100 steps per rotatable bond were used. The calculations were performed with the MacroModel program of the Schrödinger Suite [39].

2.6. Protein analysis

Yeast cell lysates were prepared as follows: A saturated cell culture was inoculated into 50 mL liquid YPD (or 2% YP-Galactose for P_{GAL1} induction) media and growing the cultures to OD_{600} 0.8–1.0. Cells were harvested, washed with sterile water and then frozen at −80°C. Lysis buffer (PBS-Tween plus Roche Complete Mini Protease Inhibitor Cocktail Tablets) was added to the cell pellet and cell breakage was accomplished by adding glass beads to equal the volume of the cell pellet, and then by vortexing for 30 seconds followed by 30 second incubation on ice. This procedure was repeated 20 times. Samples were pelleted and the resulting supernatant was recovered. Protein concentration determinations were made via the Bradford protein assay (BioRad).

AP endonuclease activity was measured by assessing the ability of cellular lysates to cleave an oligonucleotide containing the stable abasic analog, tetrahydrofuran (THF) as well as a 3′-3′ phosphodiester linkage at the 3′ end, which allowed for labeling of both ends with ^{32}P, as previously described [40–42]. This assay is specific for Apn1 activity as THF is not processed by AP lyases. Oligonucleotides are degraded *in vivo* mainly by cellular 3′–5′ exonucleases. The two 5′ ends block such degradation. In addition, the 3′-3′ phosphodiester linkage is extremely resistant to 5′ exonuclease activity. A 0.1 μg aliquot of cell lysate from each strain expressing an Apn1 variant was incubated with oligonucleotide for 15 minutes. Reactions were then loaded onto denaturing-urea polyacrilamide gels to separate the cleavage products. 0.5 μg and 1.0 μg aliquots of cell lysates from the strains overexpressing Apn1 variants from the integrated P_{GAL1} were incubated with oligo. For thermal stability assessments, 0.5μg aliquots of cell lysates from each Apn1 variant expressing strains was pre-incubated at different temperatures as previously described [43, 44]. Lysates were then incubated with oligonucleotide, and reactions were resolved as described above Dried gels were analyzed for band intensity using a TYPHOON™ phosphoImager and ImageQuant software. The % incision activity results are calculated by taking into account and correcting for labeling efficiency, which is determined by measuring the relative amounts of the 3′ and 5′ products following cleavage with the purified endonuclease IV enzyme.

For SDS-PAGE and Western blot analysis, aliquots of lysates were boiled with 6X SDS-PAGE loading buffer and samples were run on precast NU-PAGE 10%Bis-Tris minigels (Novex). Western blot analysis was performed with primary anti-TAP (1:5000) antibody (ThermoScientific) or with primary anti-Apn1 (1:200) antibody (Santa Cruz Biotechnology Inc.) Secondary HRP-conjugated anti-rabbit (1:5000) (Promega) and anti-goat (1:5000) (Santa Cruz) were employed for TAP and Apn1 detection, respectively. Blots were stripped and reprobed with anti-Pgk1 primary antibody (1:5000) (Molecular Probes) and anti-mouse secondary antibody (1:5000) (Promega) to determine the relative levels of protein loaded. Chemiluminescence was used to detect immunoreactive proteins, and protein abundance was quantified based on band intensities using ImageQuant software.

Cycloheximide chase experiments were performed as previously described [45] with the following modifications. After aliquots of cells were collected at appropriate time points following addition of cycloheximide to the growth medium, cultures were spun down and cell pellets were lysed by boiling in Laemmli urea sample buffer (63mM Tris-HCl pH 6.8, 2% SDS, 10% Glycerol, 0.01% Bromophenol blue, 5M Urea, 2% 2–Mercaptoethanol). Samples were then pelleted, and the resulting supernatants were subjected to SDS-PAGE and Western blotting with the anti-TAP antibody as described above. For each strain genotype, half-lives were estimated for each of four individual protein decay curves by fitting a straight line to the data by regression analysis to a semi-log plot of the % protein remaining with the time of incubation plotted along the x-axis using Microsoft Excel.

MG132 experiments were performed as previously described [46]. Lysates were prepared and analyzed in the manner described above for cycloheximide chase experiments.

2.7 Reverse transcriptase-PCR analysis

Cells were cultured in YPD medium and harvested as described in section 2.6. Total RNA was extracted from yeast cell pellets with the MasterPure yeast RNA purification kit from Epicentre. Reverse transcriptase (RT)-PCR was performed with the Quantitect RT-PCR kit from Qiagen. PCR optimization was performed by first determining the exponential range of the PCR reaction by analyzing PCR products at different cycle numbers by agarose gel electrophoresis. Subsequently, varying concentrations of PCR template (RT-PCR reaction) were utilized for validation. No-RT and no-RNA controls for the RT-PCR reaction were amplified by PCR and subjected to agarose gel electrophoresis alongside experimental

samples. Diagnostic PCR was performed with primers internal to the *APN1* coding sequence. PCR amplification with primers internal to the coding sequence of housekeeping gene *SRB4* was used as an internal standard.

3. Results

3.1. An Unbiased Genetic Screen Identifies MMS-Sensitive apn1 Mutants

In order to define structural components important for *in vivo* Apn1 function, we performed a small-scale unbiased, forward genetic screen for *APN1* mutations that affect cellular DNA repair capacity. Our previous studies revealed that in the absence of Apn1 its substrates can be efficiently repaired *in vivo* by two oxidative damage-specific *N*-glycosylase-associated lyases, Ntg1 and Ntg2 [28, 47–50]. For this reason the screen was carried out in a wild type background as well as a background that was both *NTG1*- and *NTG2*-deficient (*ntg1Δntg2Δ*). We sought to identify strains that displayed increased sensitivity to the DNA damaging agent methyl methanesulfonate (MMS), an alkylating chemical that induces cytotoxic and mutagenic DNA base damages [51–53]. For the initial screen we targeted a library of mutagenized fragments to the chromosomal *APN1* locus via the *delitto perfetto* cloning technique([29] and section *2.3*). All transformants were replica plated onto media containing 0.08% MMS to identify sensitive mutant clones. Following confirmation of MMS sensitivity, the *APN1* locus and upstream promoter region of 13 clones were sequenced to identify mutations (Table S2). For our analysis, we selected only clones for which resulting base changes would encode no more than two non-synonymous missense mutations (Table S2).

For further analysis, we re-introduced mutations into the chromosomal *APN1* locus in “clean” non-mutagenized backgrounds to ensure the MMS sensitivity phenotype was due only to mutations in *APN1*. We performed site-directed mutagenesis of plasmid pD0428, which contains the *APN1* coding and promoter sequences, to generate plasmids carrying specific mutant alleles. These plasmids were then used as PCR templates to construct strains expressing the mutant alleles from the endogenous *APN1* locus in non-mutagenized wild type and *ntg1Δntg2Δ* backgrounds. Newly constructed strains were tested for sensitivity to 0.08% MMS.

Sequencing of the MMS-sensitive mutants revealed that strain YDM10 contained two single nucleotide substitutions $T_{467}\rightarrow A$ and $A_{620}\rightarrow T$ in *APN1* coding region, which result in two amino acid substitutions V156E and E207V, respectively. This mutant was of particular interest because V156 is a conserved residue (Fig. 1, indicated by asterisk) for which a mutation at the corresponding residue in the *E.coli* endo IV mutant V143E has been previously shown to exhibit catalytic deficiency and decreased functional repair capacity that is independent of cellular protein levels [54]. This provided the opportunities to elucidate structure-function relationships for endonuclease IV family endonucleases and to explore how this deficiency manifests itself in eukaryotic cells. The E207V substitution is located at a non-conserved residue (Fig. 1A, indicated by star) with no readily predictable structural or functional defects based on its position within the primary amino acid sequence.

3.2. Functional Analysis of apn1-V156E, E207V Mutant

The original mutant strain identified in the screen (YDM10) containing the V156E and E207V substitutions in the *ntg1Δntg2Δ* background, was as sensitive to MMS as the strain containing an *APN1* deletion in the *ntg1Δntg2Δ* background (Fig. 2A, compare rows 3 and 4). To determine if there was contribution of second site mutations to the MMS sensitivity phenotype, we re-assessed MMS sensitivity after introduction of the $T_{467}\rightarrow A$ and $A_{620}\rightarrow T$ mutations in non-mutagenized backgrounds. In a wild type (*NTG1, NTG2*) background,

apn1-V156E, E207V (DSC517) exhibited sensitivity comparable to the *apn1Δ* strain (DSC386) (Fig. 2B, compare rows 2 and 3; Fig. 2C compare rows 2 and 5), indicating that it is a null mutant. In the *ntg1Δntg2Δ* background, which was not subjected to random mutagenesis, *apn1-V156E, E207V* (strain DSC518) exhibited MMS sensitivity similar to *apn1Δntg1Δntg2Δ* (strain DSC393) (Fig. 2B, compare rows 4 and 5), supporting the conclusion that *apn1-V156E, E207V* is a null mutation.

To determine whether the MMS-sensitivity phenotype could be attributed to either one or both mutations in *APN1*, we constructed strains expressing either *apn1-V156E* or *apn1-E207V* in the non-mutagenized *NTG1, NTG2* background and assessed their MMS sensitivity. The *apn1-V156E* mutant (DSC519) was more sensitive to 0.08% MMS than wild type, but less sensitive than *apn1Δ*(DSC386) (Fig. 2C, compare rows 1, 2 and 3). Further, the *apn1-V156E* mutant (DSC519) appeared to be less sensitive to MMS than the double mutant (DSC517) (Fig. 2C, compare rows 3 and 5), demonstrating an interaction between the two amino acids substitutions whereby the *apn1*-E207V mutation, which does not cause an apparent MMS sensitivity phenotype by itself, exacerbates the repair defect of the *apn1-V156E* mutation.

3.3. Homology Modeling Provides Insight into Structural Consequences of Amino Acid Substitutions

As there is no published high resolution structure for Apn1, our initial approach for elucidating the molecular basis of the mutant phenotypes was to employ computational molecular modeling to predict the 3D structure of Apn1 utilizing information from alignment between amino acid sequences of endo IV orthologs in bacteria, fungi and *C. elegans* and from the high resolution structure of *E. coli* endo IV (PDB ID: 1qum). Endo IV and Apn1 share 41 percent total amino acid identity. Furthermore, they share 100% amino acid identity with respect to the nine conserved metal binding amino acid residues that comprise the endo IV active site (Fig. 1A, bolded, underlined text), which together are important for DNA incision activity [20, 23, 54].

Residue V156 is located in the hydrophobic core of the protein. The substitution of V156 by glutamic acid (V156E) is predicted to disrupt hydrophobic interactions of C190. Alanine and tryptophan substitutions in the corresponding C190 residue of *E. coli* endo IV (C177) were shown to substantially affect enzyme activity [45]. In addition, V156E would form additional polar interactions, ultimately affecting hydrophobic interactions of E158 (Fig. 3A). E158 is one of the conserved residues involved in Zn^{2+} ion binding (Fig. 3A and 3B), and its mutation to glycine has been shown to substantially reduce enzyme activity in yeast [55]. Thus, we predict that the substitution of V156 for glutamic acid leads to decreased repair activity by a disruption of the catalytic site and that this structural change is responsible for the MMS sensitivity phenotype (Fig. 3A).

Based on the homology modeling predictions, residue E207 would be located on the surface of the protein at the beginning of the predicted Apn1 alpha-helix 6 (Fig. 3B), away from both the DNA binding surface and the catalytic center. The side chain of E207 would be involved in a network of intra-molecular interactions. Thus, the substitution of surface residue E207 for valine is predicted to disrupt a network of interactions that might be important for other functions, such as protein-protein interactions, but may not be substantial enough to affect functional repair capacity as measured in our assay.

3.4. AP Site Incision Activity is Compromised in apn1-V156E and apn1-V156E, E207V Mutant Cells

Based on predictions inferred from previously reported amino acid substitution mutants and homology modeling, *apn1-V156E* is expected to influence the AP site incision activity of Apn1. We measured the AP site incision activity in cellular lysates using an oligo containing the stable AP site analog, tetrahydrofuran (THF) (Fig. 4A) [40, 41]. Lysates from *apn1-E207V* mutant cells displayed incision activity comparable to wild type (Fig. 4B, compare lanes 3 and 7, and 4C), indicating that, as expected, the predicted structural changes do not impact enzyme activity. Lysates from *apn1-V156E* mutant strains exhibited a 70% reduction in incision activity compared to wild type (Fig. 4B, lanes 3 and 6), which supports the prediction that this substitution negatively affects the active site. There was no detectable incision activity in *apn1- V156E, E207V* mutant lysates (Fig. 4B, lanes 2 and 5), which is consistent with the hypothesis that the E207V substitution can further enhance the defect caused by V156E.

3.5. Cellular Levels of Apn1 V156E and Apn1 V156E, E207V Mutant Proteins are Reduced Compared to Wild Type Apn1 Levels

An alternative explanation for the decreased incision activity in cell lysates from strains expressing Apn1 variants could be variable cellular protein concentrations. Thus, we measured the steady-state levels of Apn1 protein in lysates from wild type and mutant cells. The endogenous expression of Apn1 in cell lysates is difficult to detect using antibodies against Apn1 [56–58]. We therefore integrated the tandem affinity purification (TAP) tag directly downstream of the chromosomal Apn1 locus, and then determined endogenous Apn1 protein expression levels in cell lysates using an antibody to the TAP moiety [24, 59]. It is important to note that addition of the TAP tag alone did not negatively influence functional repair capacity, as assessed by cell growth in the presence of MMS (Fig. S1).

Cellular levels of Apn1 E207V were similar to levels of the wild type protein. Apn1 V156E was detected at ~15% of wild type levels, and there was no detectable protein expression in lysates from the Apn1 V156E, E207V double mutant (Fig. 5A and 5B). Interestingly, the expression level of the mutant proteins closely correlates with the amount of incision activity within cell lysates (compare Fig. 4C and 5B). These results suggest that Apn1 V156E and Apn1 E207V are both functionally equivalent to wild type Apn1, and that reduced repair capacity in cells containing the Apn1 V156E variant may be due to decreased steady-state protein levels.

The observed decrease in cellular levels of Apn1 V156E mutant protein could be the result of a decrease at the level of either the mRNA transcript or the protein. To investigate whether there was a defect in steady-state expression of mutant *APN1* mRNA transcripts, we performed reverse transcriptase-PCR analysis. *APN1* mRNA transcript levels were similar in mutant and in wild type cells (Figure 5C), suggesting that the decrease in levels of mutant Apn1 (V156E) proteins is not caused by defects in *APN1* mRNA metabolism. Taken together, the data suggest that the *apn1-V156E* mutation plays a prominent role in the molecular phenotype of the double mutant. Therefore, we focused our attention on understanding the molecular basis of Apn1 V156E dysfunction.

3.6. Apn1-V156E Is Thermostable but Degraded More Rapidly than Wild Type Apn1

The decrease in steady-state expression level of Apn1 protein in *apn1-V156E* mutants could be due to a decrease in protein production and/or an increase in protein degradation. The former possibility would suggest that mutant Apn1 V156E polypeptide can be produced but may be translated inefficiently. This is unlikely because there are no mutations in the regulatory region upstream of the *APN1* locus in this mutant (data not shown). Moreover,

the $T_{467}\rightarrow A$ base substitution in the *apn1-V156E* mutant results in usage of the preferred glutamic acid codon in yeast (GAA versus GAG) [60], ruling out a codon bias mechanism. A more plausible explanation for the decreased mutant protein level is that the V156E substitution leads to degradation by causing the protein to be unstable. To test this prediction, we assessed the thermostability of Apn1 variants within cellular lysates. Following pre-incubation at increasing temperatures, lysates from wild type and Apn1 mutant cells displayed similar resistance to heat treatment with respect to AP incision activity, with the loss of activity for each lysate occurring at 72°C (Fig. 6A). This suggests that Apn1 V156E, when in its functional conformation, is not less stable than wild type Apn1.

Missense substitution mutations can also impair the proper folding of a protein into its mature form, often leading to degradation. We predicted that the V156E substitution causes less of the functional protein to accumulate due to accelerated elimination from the cell. To determine whether mutant Apn1 V156E protein is degraded more quickly than wild type Apn1, we determined the half-life for the protein variants by employing the translational inhibitor cycloheximide and measuring protein levels via SDS-PAGE and Western blot analysis on extracts from cells expressing C-terminal TAP-tag versions of Apn1. Following addition of cycloheximide to the culture medium, the amount of Apn1 V156E protein decreased faster than wild type protein (Fig. 6B and 6C). While the half-life of wild type Apn1 was estimated to be ~90 minutes, the half-life of V156E was reduced by ~3-fold to an estimated ~30 minutes (Fig. 6D). To determine whether proteosome function was involved in regulating the turnover of Apn1 V156E we employed the proteosome inhibitor MG132 in combination with cycloheximide and performed a chase analysis experiment. Inhibition of proteasome function led to accumulation of the wild type but not the variant protein in cells (Fig. 6E). Our results suggest that, while wild type protein turnover may be regulated by the proteosome, cells use an alternative pathway to eliminate the mutant Apn1 V156E protein. Taken together, the data support the prediction that the mutant protein is degraded more rapidly than wild type, leading to the observed decrease in steady-state levels of Apn1 V156E.

3.7. Overexpression of apn1-V156E Restores Cellular DNA Repair Activity

Since the AP site incision activity of Apn1 variants correlates with the steady-state protein level in cell lysates, we hypothesized that increased cellular Apn1V156E levels would result in increased AP site incision activity. To overexpress *APN1*, we integrated the galactose-inducible *GAL1* promoter upstream of the chromosomal *APN1* open reading frame and induced expression in galactose-containing growth medium. We examined the galactose-induced expression levels of the Apn1 variants in cell lysates via SDS-PAGE and Western blot analysis using the anti-Apn1 antibody. (Fig. 7A). Galactose-induced overexpression of wild type Apn1 and both variants lead to production of comparable amounts of protein, although Apn1 V156E accumulated to lower levels.

We next decided to measure the difference in endogenous and galactose-induced levels of Apn1. To estimate the relative overexpression levels of Apn1 variants versus endogenous wild type Apn1 expression levels, we first integrated a P_{GAL1}-TAP construct directly upstream of the chromosomal Apn1 locus. We then compared galactose-induced overexpression levels of TAP-Apn1 and TAP-Apn1-V156E (C-terminal tags) to that of Apn1-TAP expressed from the endogenous *APN1* promoter at the chromosomal locus using the anti-TAP antibody. Compared to normal Apn1 protein levels, galactose-induced *APN1* overexpression resulted in an ~30-fold increase in protein levels (Fig. 7B and 7C). The difference in protein levels in wild type without galactose induction and P_{GAL1} – *apn1-V156E* strain subjected to galactose-induced overexpression was barely distinguishable (Fig. 7B, first and third lanes, and 7C).

To test the prediction that the Apn1 V156E retains catalytic function, we measured AP incision activity in lysates from cells overexpressing the mutant alleles. In lysates containing increased levels of Apn1 V156E following galactose-induced expression, incision activity was increased compared to the level of activity in lysates from cells expressing *apn1*-V156E from the endogenous *APN1* promoter (Fig. 7D, lanes 4 and 7). In addition, the incision activity in lysates harboring overexpressed Apn1 V156E was comparable to incision activity in lysates from cells expressing Apn1 from the endogenous promoter (Fig. 7D, lanes 4 and 6). Notably, the *E. coli* endo IV variant V143E previously reported by Jilani, *et al.* did not display catalytic activity upon overexpression in cell lysates [54]. These results indicate that while the Apn1 V156E substitution leads to decreased accumulation of native protein within the cell, this protein variant retains catalytic activity comparable to wild type Apn1.

To determine whether overexpression of *apn1-V156E* could restore *in vivo* DNA repair capacity, we assessed growth of cells expressing Apn1 V156E under the control of the *GAL1* promoter in the presence of galactose and MMS. The MMS sensitivity of cells overexpressing Apn1 V156E appeared to be similar to the MMS sensitivity of the cells expressing endogenous levels of wild type Apn1. Galactose-induced overexpression of *apn1-V156E* leads to accumulation of mutant protein at levels similar to endogenous wild type levels under non-induction conditions. (Fig. 7E, compare rows 1 and 6). Galactose-induced overexpression of wild type *APN1* and the functionally equivalent *apn1-E207V* led to inability to grow in the presence of MMS (Fig. 7E, rows 5 and 7). This is presumably due to accumulation of toxic BER intermediates upon increased repair activity [61]. Nonetheless, accumulation of Apn1 V156E at increased concentrations functionally restored cellular DNA repair capacity.

4. Discussion

The absence of major AP endonuclease function in cells results in inability to repair a large subset of spontaneous and genotoxic agent-induced DNA damage [62]. In humans, genetic defects in APE1 are associated with diseases including cancer, but the precise molecular mechanisms related to pathology are largely unknown [9–11, 63]. A major challenge to elucidating such mechanisms is the complexity of studies in human cells including inter-individual genetic variability, cell-type specific gene expression and the multiple DNA repair-independent cellular functions of APE1.

We studied genetic defects in Apn1, the major AP endonuclease in *Saccharomyces cerevisiae*, since the basic biochemical mechanisms of BER are highly conserved from yeast to humans. We initiated our studies in a functionally relevant context by directly screening random mutations at the chromosomal *APN1* locus to discover aspects of structure that are important for *in vivo* repair activity. We identified amino acid variant Apn1 V156E, which renders cells sensitive to growth in the presence of MMS. The V156E amino acid substitution is homologous to the previously characterized endo IV V143E that also confers MMS sensitivity [54]. Thus, this study represents the independent identification of an amino acid substitution at an evolutionally conserved residue outside the active site, but within the hydrophobic core, that disrupts Apn1 biological function. The endo IV V143E mutant displayed defective repair capacity independent of its steady-state expression level [54]. Therefore, along with the structural information from *E. coli* endo IV, we predicted that the Apn1 V156E substitutions would cause catalytic deficiency via disruption of the important active site residue, E158 [55]. Unlike the *E. coli* V143E substitution, Apn1 V156E retained catalytic ability and exhibited normal levels of repair when expressed at increased steady-state levels. Surprisingly, the repair defect of this amino acid change could not be attributed to impaired catalytic function, but was instead due to decreased cellular protein levels compared to wild type Apn1. Although the specific mechanism that targets Apn1 V156E for

elimination from the cell are unknown, the substitution of the hydrophobic valine residue for the hydrophilic glutamic acid residue within the hydrophobic core suggests that the V156E substitution may cause protein instability and/or a defect in protein folding. It will be important to elucidate the precise molecular defects resulting from this particular amino acid substitution in future studies.

Our study revealed different molecular phenotypes for the mutant yeast Apn1 versus the homologous mutant *E. coli* endo IV, indicating that endo IV V143 and Apn1 V156 may play somewhat different roles in endonuclease structure. The predictive potential of our analysis was limited by the fact that no high-resolution structure of Apn1 has been reported to date. Nonetheless, apparent differences between Apn1 and endo IV, however subtle, can be exploited to further elucidate structure-function relationships for this family of AP endonucleases.

A common readout currently used in the field to measure protein dysfunction caused by missense mutations in APE1 is the catalytic activity of purified enzymes, which has only been validated for a small number of variants [10, 11]. While it has been proposed that alterations in repair enzymes likely to affect repair capacity will occur in the catalytic domain of the protein [9], our study and various *in silico* analyses of APE1 missense variants [11, 12, 64] provide evidence that this may not always be the case. Disruption of Apn1 active site residues E158 and D192 has been shown to severely affect catalytic capability and cellular repair capacity while leaving expression level intact [55]. Our results reveal that the opposite can be true: disruption of a residue outside the active site of Apn1 can also affect repair capacity by a mechanism that does not affect enzyme activity, but instead appears to disrupt folding and/or stability. Studies utilizing the high-resolution structure of APE1 to computationally predict the impact of amino acid substitutions found in the human population have identified many changes not expected to directly affect DNA binding, catalytic activity or protein-protein interactions [11, 12]. Some of these changes are expected to impact protein stability, ligand binding, or hydrophobicity [11, 12]. We predict that such perturbations in APE1 biology could have as significant an effect on repair capacity as missense substitutions in known functional domains. Whether or not these mutants affect repair capacity *in vivo* is yet to be determined, but based on our unexpected findings they should be prioritized for experimental validation of function. Such mutant proteins, especially those that may be associated with pathological conditions, may be candidates for pharmacological chaperone therapy, which seeks to specifically target unstable and/or misfolded mutant proteins to promote stabilization of the functional structure [65, 66].

The central role Apn1 plays in the repair of DNA damage is underscored by the fact that yeast cells completely lacking the major AP endonuclease display a mutator phenotype and are extraordinarily sensitive to oxidative and alkylation DNA damaging agents [67]. The results reported here illustrate that change in the cellular protein level of Apn1 and Apn1 variants above or below a critical concentration can substantially influence repair capacity. Such imbalances in other BER proteins are known to be mutagenic as exemplified by studies in yeast where overexpression of *MAG1* increases spontaneous mutation rates by several hundred-fold [68]. In mice heterozygous for the gene encoding the APE1 mouse homolog *Apex*, steady-state expression levels are reduced by 50%, which is accompanied by increased frequency of spontaneous tumor development [69]. Our finding that reduced Apn1 V156E mutant protein levels lead to MMS sensitivity, supports a potential role for similar APE1 defects in cancer development according to a previously proposed model whereby spontaneous damage combined with BER defects over time lead to accumulation of mutations, genomic instability and eventually cellular transformation [70]. Accelerated protein degradation is an important mechanism for loss of function caused by missense

mutations outside known functional regions of a protein [71]. Our studies have important implications for the use of simple model genetic organisms such as yeast to elucidate the functional role of missense SNPs predicted to influence DNA repair capacity and that are associated with risk for human disease development.

Supplementary Material

Refer to Web version on PubMed Central for supplementary material.

Acknowledgments

We are very grateful to Alexander Fedotov and Drs. Xiaodong Cheng, Kirill Lobachev, Rossella Marullo, Erica Werner and Keith Wilkinson for critical reading of the manuscript and helpful discussions. This work was supported by NIEHS grant ES011163.

References

1. Haracska L, Unk I, Johnson RE, Johansson E, Burgers PMJ, Prakash S, Prakash L. Roles of yeast DNA polymerases δ and ζ and of Rev1 in the bypass of abasic sites. Genes & Development. 2001; 15:945–954. [PubMed: 11316789]
2. Yu S-L, Lee S-K, Johnson RE, Prakash L, Prakash S. The Stalling of Transcription at Abasic Sites Is Highly Mutagenic. Molecular and Cellular Biology. 2003; 23:382–388. [PubMed: 12482989]
3. Lawrence AL. Apurinic sites as mutagenic intermediates. Cell. 1985; 40:483–484. [PubMed: 2982494]
4. Lindahl T. Instability and decay of the primary structure of DNA. Nature. 1993; 362:709–715. [PubMed: 8469282]
5. Nakamura J, Walker VE, Upton PB, Chiang S-Y, Kow YW, Swenberg JA. Highly Sensitive Apurinic/Apyrimidinic Site Assay Can Detect Spontaneous and Chemically Induced Depurination under Physiological Conditions. Cancer Research. 1998; 58:222–225. [PubMed: 9443396]
6. Duncan J, Hamilton L, Friedberg EC. Enzymatic degradation of uracil-containing DNA. II. Evidence for N-glycosidase and nuclease activities in unfractionated extracts of Bacillus subtilis. J Virol. 1976; 19:338–345. [PubMed: 822172]
7. Lindahl T. New class of enzymes acting on damaged DNA. Nature. 1976; 259:64–66. [PubMed: 765833]
8. Chen DS, Herman T, Demple B. Two distinct human DNA diesterases that hydrolyze 3′-blocking deoxyribose fragments from oxidized DNA. Nucleic Acids Research. 1991; 19:5907–5914. [PubMed: 1719484]
9. Mohrenweiser HW, Wilson DM III, Jones IM. Challenges and complexities in estimating both the functional impact and the disease risk associated with the extensive genetic variation in human DNA repair genes. Mutation Research/Fundamental and Molecular Mechanisms of Mutagenesis. 2003; 526:93–125.
10. Wilson DM III, Kim D, Berquist BR, Sigurdson AJ. Variation in base excision repair capacity. Mutation Research/Fundamental and Molecular Mechanisms of Mutagenesis. 2011; 711:100–112.
11. Hadi MZ, Coleman MA, Fidelis K, Mohrenweiser HW, Wilson DM III. Functional characterization of Ape1 variants identified in the human population. Nucleic Acids Research. 2000; 28:3871–3879. [PubMed: 11024165]
12. Yu ET, Hadi MZ. Bioinformatic processing to identify single nucleotide polymorphism that potentially affect Ape1 function. Mutation Research/Genetic Toxicology and Environmental Mutagenesis. 2011; 722:140–146.
13. Paul W, Doetsch RPC. The enzymology of apurinic/apyrimidinic endonucleases. Mutation Research. 1990; 236:173–201. [PubMed: 1697933]
14. Tomicic M, Eschbach E, Kaina B. Expression of yeast but not human apurinic/apyrimidinic endonuclease renders Chinese hamster cells more resistant to DNA damaging agents. Mutation Research/DNA Repair. 1997; 383:155–165.

15. He Y-H, Wu M, Kobune M, Xu Y, Kelley MR, Martin WJ II. Expression of Yeast Apurinic/Apyrimidinic Endonuclease (APN1) Protects Lung Epithelial Cells From Bleomycin Toxicity. Am J Respir Cell Mol Biol. 2001; 25:692–698. [PubMed: 11726394]
16. Fung H, Demple B. A Vital Role for Ape1/Ref1 Protein in Repairing Spontaneous DNA Damage in Human Cells. Molecular Cell. 2005; 17:463–470. [PubMed: 15694346]
17. Tell G, Quadrifoglio F, Tiribelli C, Kelley MR. The many functions of APE1/Ref-1: not only a DNA repair enzyme. Antioxidants & redox signaling. 2009; 11:601–620. [PubMed: 18976116]
18. Vascotto C, Fantini D, Romanello M, Cesaratto L, Deganuto M, Leonardi A, Radicella JP, Kelley MR, D'Ambrosio C, Scaloni A, Quadrifoglio F, Tell G. APE1/Ref-1 Interacts with NPM1 within Nucleoli and Plays a Role in the rRNA Quality Control Process. Molecular and Cellular Biology. 2009; 29:1834–1854. [PubMed: 19188445]
19. Kuninger DT, Izumi T, Papaconstantinou J, Mitra S. Human AP-endonuclease 1 and hnRNP-L interact with a nCaRE-like repressor element in the AP-endonuclease 1 promoter. Nucleic Acids Research. 2002; 30:823–829. [PubMed: 11809897]
20. Hosfield DJ, Guan Y, Haas BJ, Cunningham RP, Tainer JA. Structure of the DNA Repair Enzyme Endonuclease IV and Its DNA Complex: Double-Nucleotide Flipping at Abasic Sites and Three-Metal-Ion Catalysis. Cell. 1999; 98:397–408. [PubMed: 10458614]
21. Mol CD, Izumi T, Mitra S, Tainer JA. DNA-bound structures and mutants reveal abasic DNA binding by APE1 DNA repair and coordination. Nature. 2000; 403:451–456. [PubMed: 10667800]
22. Mol CD, Hosfield DJ, Tainer JA. Abasic site recognition by two apurinic/apyrimidinic endonuclease families in DNA base excision repair: the 3′ ends justify the means. Mutation Research/DNA Repair. 2000; 460:211–229.
23. Garcin ED, Hosfield DJ, Desai SA, Haas BJ, Bjoras M, Cunningham RP, Tainer JA. DNA apurinic-apyrimidinic site binding and excision by endonuclease IV. Nat Struct Mol Biol. 2008; 15:515–522. [PubMed: 18408731]
24. Griffiths LM, Swartzlander D, Meadows KL, Wilkinson KD, Corbett AH, Doetsch PW. Dynamic Compartmentalization of Base Excision Repair Proteins in Response to Nuclear and Mitochondrial Oxidative Stress. Mol Cell Biol. 2009; 29:794–807. [PubMed: 19029246]
25. Schiestl RH, Gietz RD. High efficiency transformation of intact yeast cells using single stranded nucleic acids as a carrier. Current Genetics. 1989; 16:339–346. [PubMed: 2692852]
26. Sikorski RS, Hieter P. A System of Shuttle Vectors and Yeast Host Strains Designed for Efficient Manipulation of DNA in Saccharomyces cerevisiae. Genetics. 1989; 122:19–27. [PubMed: 2659436]
27. Hong Ma SK, Peter Schatz J, Botstein David. Plasmid Construction by Homologous Recombination in Yeast. Gene. 1987; 58:201–216. [PubMed: 2828185]
28. Degtyareva NP, Chen L, Mieczkowski P, Petes TD, Doetsch PW. Chronic Oxidative DNA Damage Due to DNA Repair Defects Causes Chromosomal Instability in Saccharomyces cerevisiae. Mol Cell Biol. 2008; 28:5432–5445. [PubMed: 18591251]
29. Storici, F.; Resnick, MA. The Delitto Perfetto Approach to In Vivo Site[hyphen (true graphic)]Directed Mutagenesis and Chromosome Rearrangements with Synthetic Oligonucleotides in Yeast. In: Judith, LC.; Paul, M., editors. Methods in Enzymology. Academic Press; 2006. p. 329-345.
30. Juili L, Lin-Goerke DJR, John Burczak D. PCR-Based Random Mutagenesis Using Manganese and Reduced dNTP Concentration. BioTechniques. 1997; 23:409–412. [PubMed: 9298207]
31. Puig O, Caspary F, Rigaut G, Rutz B, Bouveret E, Bragado-Nilsson E, Wilm M, Séraphin B. The Tandem Affinity Purification (TAP) Method: A General Procedure of Protein Complex Purification. Methods. 2001; 24:218–229. [PubMed: 11403571]
32. The UniProt Consortium. Reorganizing the protein space at the Universal Protein Resource (UniProt). Nucleic Acids Research. 2012; 40:D71–D75. [PubMed: 22102590]
33. Larkin MA, Blackshields G, Brown NP, Chenna R, McGettigan PA, McWilliam H, Valentin F, Wallace IM, Wilm A, Lopez R, Thompson JD, Gibson TJ, Higgins DG. Clustal W and Clustal X version 2.0. Bioinformatics. 2007; 23:2947–2948. [PubMed: 17846036]
34. Sali A, Blundell TL. Comparative Protein Modelling by Satisfaction of Spatial Restraints. Journal of Molecular Biology. 1993; 234:779–815. [PubMed: 8254673]

35. Impact, version 5.5. Schrödinger, LLC; New York, NY: 2005.
36. Epik, version 2.0. Schrödinger, LLC; New York, NY: 2009.
37. Prime, version 2.1. Schrödinger, LLC; New York, NY: 2009.
38. Maestro, version 9.2. Schrödinger, LLC; New York, NY: 2011.
39. MacroModel, version 9.9. Schrödinger, LLC; New York, NY: 2011.
40. Muniz JF, McCauley L, Scherer J, Lasarev M, Koshy M, Kow YW, Nazar-Stewart V, Kisby GE. Biomarkers of oxidative stress and DNA damage in agricultural workers: A pilot study. Toxicology and Applied Pharmacology. 2008; 227:97–107. [PubMed: 18086483]
41. Kisby GE, Kohama SG, Olivas A, Churchwell M, Doerge D, Spangler E, Cabo Rd, Ingram DK, Imhof B, Bao G, Kow YW. Effect of caloric restriction on base-excision repair (BER) in the aging rat brain. Experimental Gerontology. 2010; 45:208–216. [PubMed: 20005284]
42. Johnson AW, Demple B. Yeast DNA diesterase for 3′-fragments of deoxyribose: purification and physical properties of a repair enzyme for oxidative DNA damage. Journal of Biological Chemistry. 1988; 263:18009–18016. [PubMed: 3056935]
43. Winterbourn CC, Domigan NM, Broom JK. Decreased thermal stability of red blood cellglu100→gly superoxide dismutase from a family with amyotrophic lateral sclerosis. FEBS Letters. 1995; 368:449–451. [PubMed: 7635196]
44. Horton JR, Sawada K, Nishibori M, Zhang X, Cheng X. Two Polymorphic Forms of Human Histamine Methyltransferase: Structural, Thermal, and Kinetic Comparisons. Structure. 2001; 9:837–849. [PubMed: 11566133]
45. Katzmann, DJ.; Wendland, B. Analysis of Ubiquitin-Dependent Protein Sorting Within the Endocytic Pathway in Saccharomyces cerevisiae. In: Raymond, JD., editor. Methods in Enzymology. Academic Press; 2005. p. 192-211.
46. Liu C, Apodaca J, Davis LE, Rao H. Proteasome inhibition in wild-type yeast *Saccharomyces cerevisiae* cells. BioTechniques. 2007; 42:158–162. [PubMed: 17373478]
47. Evert BA, Salmon TB, Song B, Jingjing L, Siede W, Doetsch PW. Spontaneous DNA Damage in Saccharomyces cerevisiae Elicits Phenotypic Properties Similar to Cancer Cells. Journal of Biological Chemistry. 2004; 279:22585–22594. [PubMed: 15020594]
48. Salmon TB, Evert BA, Song B, Doetsch PW. Biological consequences of oxidative stress-induced DNA damage in Saccharomyces cerevisiae. Nucleic Acids Research. 2004; 32:3712–3723. [PubMed: 15254273]
49. Swanson RL, Morey NJ, Doetsch PW, Jinks-Robertson S. Overlapping Specificities of Base Excision Repair, Nucleotide Excision Repair, Recombination, and Translesion Synthesis Pathways for DNA Base Damage in Saccharomyces cerevisiae. Mol Cell Biol. 1999; 19:2929–2935. [PubMed: 10082560]
50. Hanna M, Chow BL, Morey NJ, Jinks-Robertson S, Doetsch PW, Xiao W. Involvement of two endonuclease III homologs in the base excision repair pathway for the processing of DNA alkylation damage in Saccharomyces cerevisiae. DNA Repair. 2004; 3:51–59. [PubMed: 14697759]
51. Boiteux S, Laval J. Mutagenesis by alkylating agents: Coding properties for DNA polymerase of poly (dC) template containing 3-methylcytosine. Biochimie. 1982; 64:637–641. [PubMed: 6814512]
52. Loechler CLGEL, Essigmann JM. In vivo mutagenesis by 06-methylguanine built into a unique site in a viral genome. Proceedings of the National Academy of Sciences. 1984; 81:6271–6275.
53. Larson K, Sahm J, Shenkar R, Strauss B. Methylation-induced blocks to in vitro DNA replication. Mutation Research/Fundamental and Molecular Mechanisms of Mutagenesis. 150:77–84.
54. Yang X, Tellier P, Masson J-Y, Vu T, Ramotar D. Characterization of Amino Acid Substitutions That Severely Alter the DNA Repair Functions of Escherichia coli Endonuclease IV†. Biochemistry. 1999; 38:3615–3623. [PubMed: 10090748]
55. Jilani A, Vongsamphanh R, Leduc A, Gros L, Saparbaev M, Ramotar D. Characterization of Two Independent Amino Acid Substitutions that Disrupt the DNA Repair Functions of the Yeast Apn1†. Biochemistry. 2003; 42:6436–6445. [PubMed: 12767225]

56. Ramotar D, Kim C, Lillis R, Demple B. Intracellular localization of the Apn1 DNA repair enzyme of Saccharomyces cerevisiae. Nuclear transport signals and biological role. Journal of Biological Chemistry. 1993; 268:20533–20539. [PubMed: 7690756]
57. Vongsamphanh R, Fortier P-K, Ramotar D. Pir1p Mediates Translocation of the Yeast Apn1p Endonuclease into the Mitochondria To Maintain Genomic Stability. Mol Cell Biol. 2001; 21:1647–1655. [PubMed: 11238901]
58. Popoff SC, Spira AI, Johnson AW, Demple B. Yeast structural gene (APN1) for the major apurinic endonuclease: homology to Escherichia coli endonuclease IV. Proceedings of the National Academy of Sciences of the United States of America. 1990; 87:4193–4197. [PubMed: 1693433]
59. Ghaemmaghami S, Huh W-K, Bower K, Howson RW, Belle A, Dephoure N, O'Shea EK, Weissman JS. Global analysis of protein expression in yeast. Nature. 2003; 425:737–741. [PubMed: 14562106]
60. SGD Project "Saccharomyces Genome Database". 1999.
61. Rusyn I, Fry RC, Begley TJ, Klapacz J, Svensson JP, Ambrose M, Samson LD. Transcriptional Networks in *S. cerevisiae* Linked to an Accumulation of Base Excision Repair Intermediates. PLoS ONE. 2007; 2:e1252. [PubMed: 18043759]
62. Zharkov D. Base excision DNA repair. Cellular and Molecular Life Sciences. 2008; 65:1544–1565. [PubMed: 18259689]
63. Frosina G. Commentary: DNA base excision repair defects in human pathologies. Free Radical Research. 2004; 38:1037–1054. [PubMed: 15512792]
64. Doss CGP, NagaSundaram N. Investigating the Structural Impacts of I64T and P311S Mutations in APE1-DNA Complex: A Molecular Dynamics Approach. PLoS ONE. 2012; 7:e31677. [PubMed: 22384055]
65. Ringe D, Petsko G. Q&A: What are pharmacological chaperones and why are they interesting? Journal of Biology. 2009; 8:80. [PubMed: 19833004]
66. Bernier V, Lagacé M, Bichet DG, Bouvier M. Pharmacological chaperones: potential treatment for conformational diseases. Trends in Endocrinology & Metabolism. 2004; 15:222–228. [PubMed: 15223052]
67. Ramotar D, Popoff SC, Gralla EB, Demple B. Cellular role of yeast Apn1 apurinic endonuclease/3′-diesterase: repair of oxidative and alkylation DNA damage and control of spontaneous mutation. Mol Cell Biol. 1991; 11:4537–4544. [PubMed: 1715020]
68. Glassner BJ, Rasmussen LJ, Najarian MT, Posnick LM, Samson LD. Generation of a strong mutator phenotype in yeast by imbalanced base excision repair. Proceedings of the National Academy of Sciences. 1998; 95:9997–10002.
69. Meira LB, Devaraj S, Kisby GE, Burns DK, Daniel RL, Hammer RE, Grundy S, Jialal I, Friedberg EC. Heterozygosity for the Mouse Apex Gene Results in Phenotypes Associated with Oxidative Stress. Cancer Research. 2001; 61:5552–5557. [PubMed: 11454706]
70. Nemec AA, Wallace SS, Sweasy JB. Variant base excision repair proteins: Contributors to genomic instability. Seminars in Cancer Biology. 2010; 20:320–328. [PubMed: 20955798]
71. Waters PJ. Degradation of Mutant Proteins, Underlying "Loss of Function" Phenotypes, Plays a Major Role in Genetic Disease. Current Issues in Molecular Biology. 2001; 3:57–65. [PubMed: 11488412]

Highlights

- Apn1 variant modeled as a catalytic mutant retains DNA repair activity when overexpressed
- Accelerated enzyme degradation, not catalytic deficiency, causes impairment of DNA repair
- A Simple model system provides insight for elucidating function of disease-associated hAPE1 SNPs

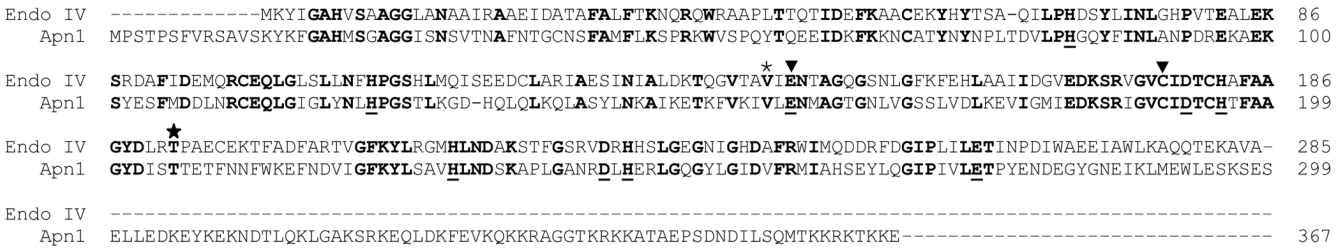

Figure 1. Amino acid alignment of *E. coli* endo IV and *S. cerevisiae* Apn1

Conserved residues indicated with bold font. Zn^{2+}-binding active site residues indicated in bold font and underlined. Residues V156 and E207 indicated by an asterisk and a star, respectively. Residues predicted to be affected by the V156E substitution are indicated with arrow heads.

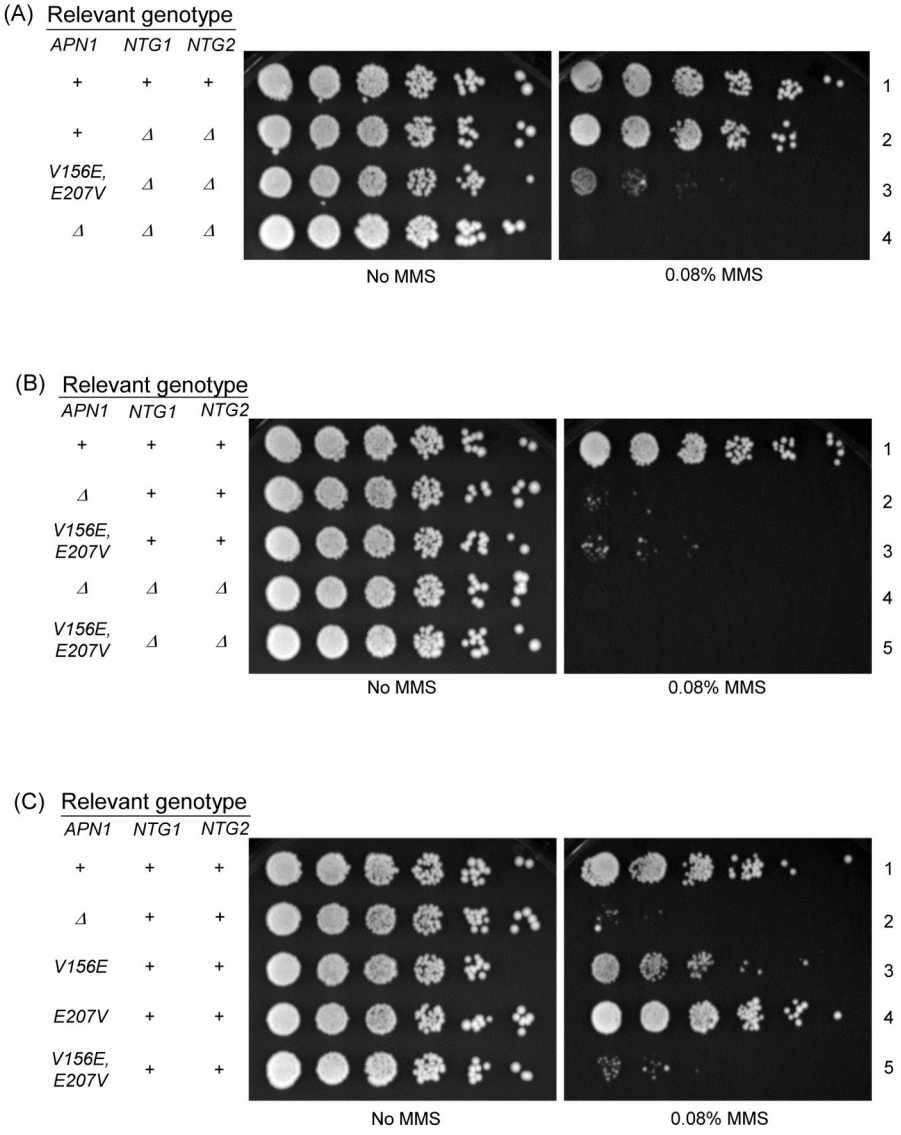

Figure 2. MMS sensitivity of *apn1* mutant strains

5-fold serial dilutions of cells were spotted onto YPD plates containing 0.08% MMS. The genotypes with respect to *APN1, NTG1* and *NTG2* are designated +: wild type, *Δ*: deletion, or by amino acid substitution. **(A)** MMS sensitivity of the original mutant strain YDM10. Row 1: *APN1* (DSC320), Row 2: *ntg1Δ ntg2Δ* (DSC386), Row 3: *apn1-V156E, E207V ntg1Δ ntg2Δ* (YDM10), Row 4: *apn1Δ ntg1Δ ntg2Δ* (DSC393). **(B)** MMS sensitivity of *apn1-V156E, E207V* in non-mutagenized backgrounds. Row 1: *APN1* (DSC320); Row 2: *apn1Δ* (DSC393); Row 3: *apn1-V156E, E207V* (DSC517), Row 4: *apn1Δntg1Δntg2Δ* (DSC378); Row 5: *apn1-V156E, E207 Vntg1Δ ntg2Δ*(DSC518). **(C)** MMS sensitivity of single mutants *apn1-V156E* and *apn1-E207V*, and double mutant *apn1-V156E, E207V* in non-mutagenized background. Row 1: *APN1* (DSC320); Row 2: *apn1Δ* (DSC326); Row 3: *apn1-V156E* (DSC519); Row 4: *apn1-E207V* (DSC520); Row 5: *apn1-V156E, E207V* (DSC517).

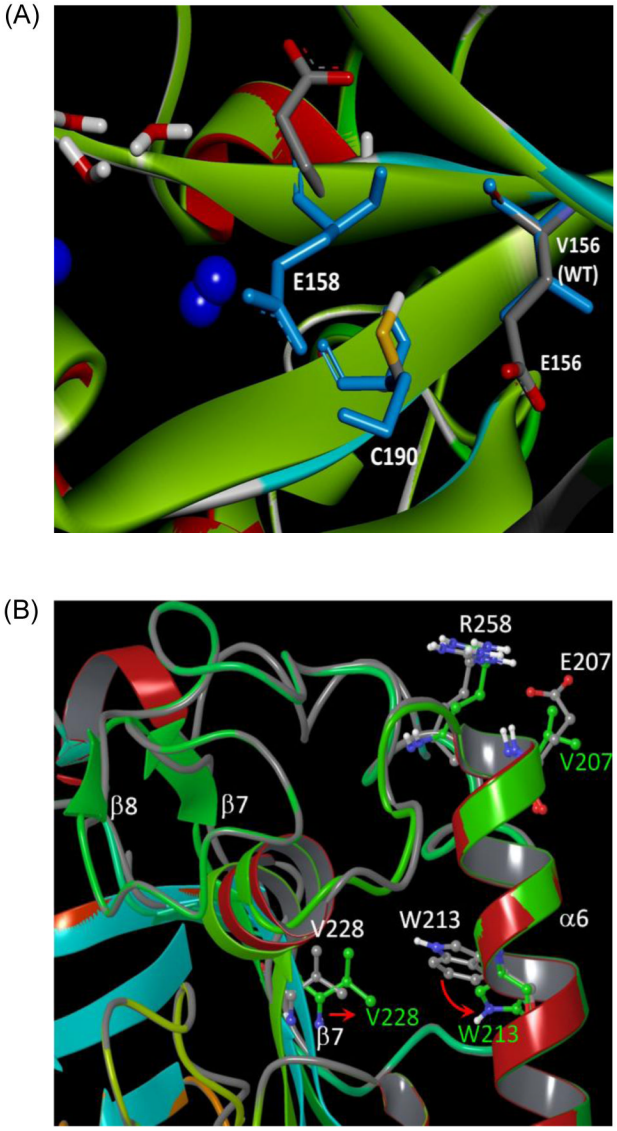

Figure 3. Homology modeling of Apn1

(A) Superimposed structures of the predicted models of wild type and Apn1 V156E, E207V zoomed in on the V156 region. Green: wild type backbone, Blue: wild type side chains, Red: mutant α-helices, Grey: mutant loops, Teal: mutant β-sheets, Blue spheres: Zn^{2+}ions. **(B)** Superimposed structures of the predicted models of wild type and Apn1V156E, E207V zoomed in on the E207 region. Grey ribbons :wild type backbone, Grey side chains: wild type residues, Green ribbons: wild type backbone, Green side chains: residues in the mutant, Red: wild type α-helices, Teal: wild type β-sheets.

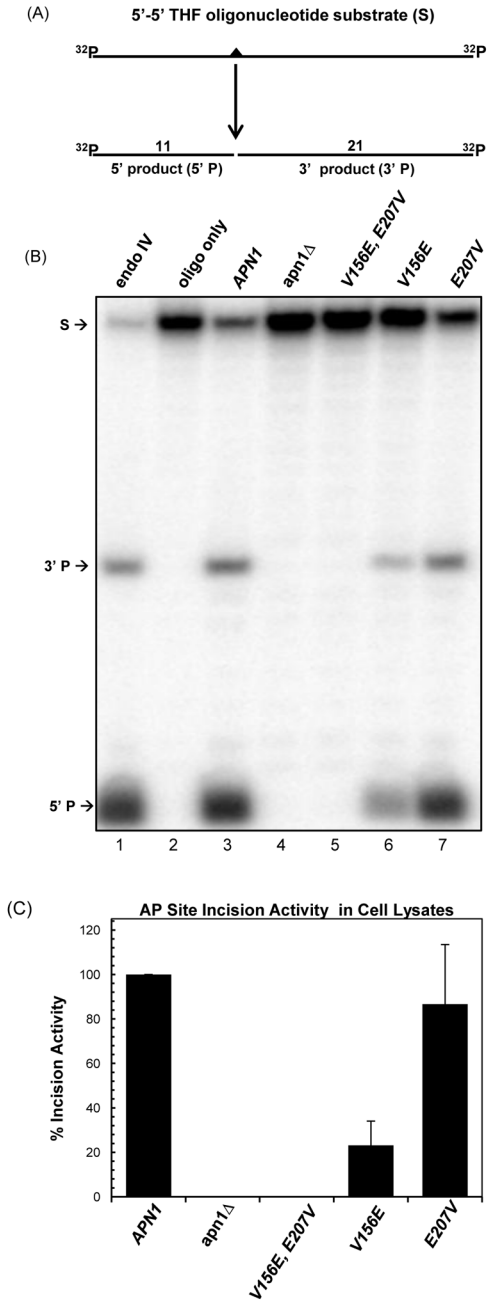

Figure 4. Measurement of AP site incision activity in cell lysates containing Apn1 variant proteins

(A) Schematic diagram of oligonucleotide substrate used in AP endonuclease incision assay. The oligonucleotide substrate contains a tetrahydrofuran (THF) site and is labeled at both ends with ^{32}P. Expected cleavage product sizes are denoted. **(B)** Representative image of oligo incision assay. AP endonuclease activity was determined by assessing the extent of cleavage following incubation of oligo with 1.0 μg aliqots of lysates from cells of the indicated *APN1* genotypes. No lysate was added to the "oligo only" reaction. Incubation of purified recombinant endo IV with oligo served as a positive control. Incision products were resolved on a polyacrilamide urea-denaturing gel and visualized via phosphorimager.

Arrows indicate the positions of the oligonucleotide substrate (S), the 3′ cleavage product (3′ P), and the 5′ cleavage product (5′ P). **(C)** Quantification of AP incision activity from three independent experiments. Error bars represent standard deviation.

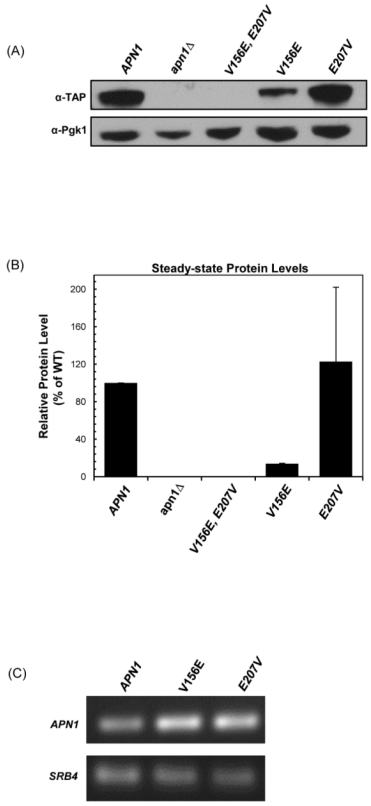

Figure 5. Quantification of endogenous Apn1 protein and *APN1* mRNA levels

(A) Detection of endogenous protein levels in cells with TAP-tagged Apn1 variants. 50 μg of lysates from cells containing C-terminal TAP fusions of the wild type and variant Apn1 proteins were resolved by SDS-PAGE and subjected to Western blot analysis by probing with anti-TAP antibody. Blots were reprobed with anti-Pgk1 antibody to determine the relative levels of protein loaded. **(B)** Quantification of protein levels from three independent experiments. Error bars represent standard deviation. **(C)** Quantification of *APN1* mRNA levels. Total RNA from wild type and mutant strains was subjected to reverse transcriptase (RT)-PCR. RT-PCR products were subjected to PCR analysis and resolved on a 1.2% agarose gel stained with ethidium bromide for visualization. Gel image is representative of at least three independent experiments.

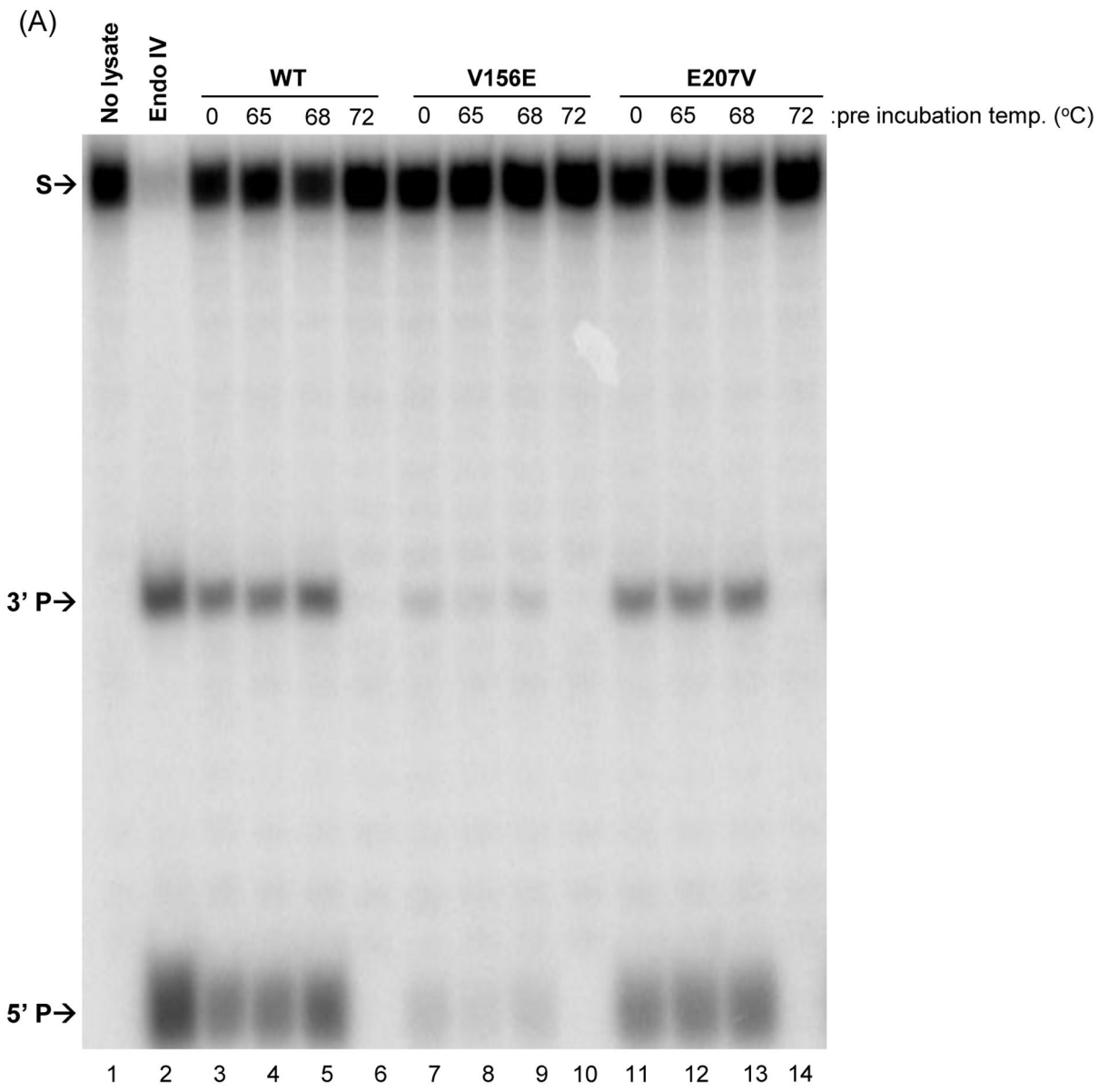

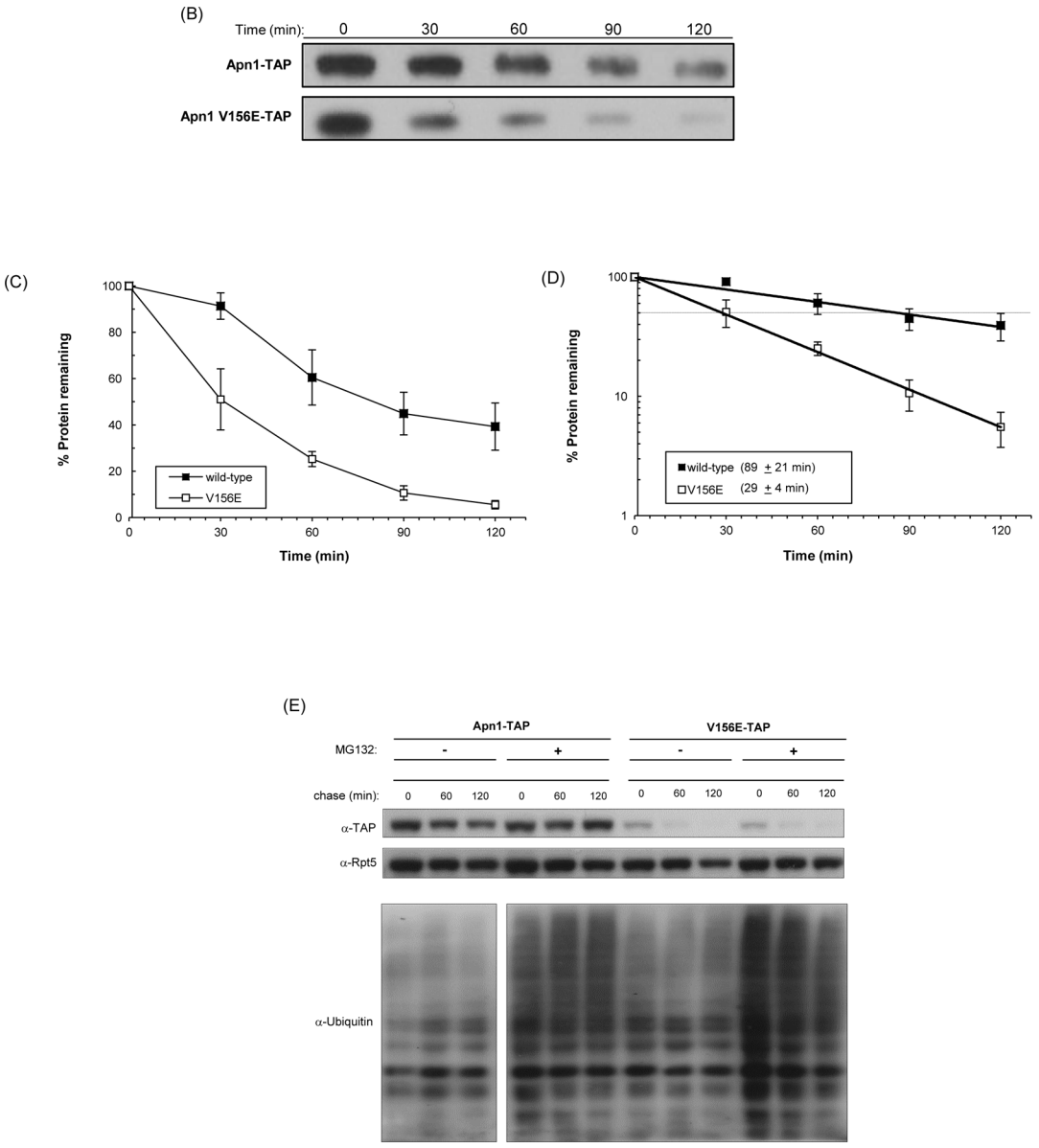

Figure 6. Thermostability and degradation of Apn1 variant proteins

(A) Thermal stability incision activity assay. Aliquots of 0.5 μg of cellular lysates from the indicated strains were pre-incubated at 0° C, 65° C, 68°C or 72° C for thirty minutes. Lysates were then incubated with a THF-containing oligonucleotide substrate labeled at both ends with ^{32}P. Reaction products were resolved on a polyacrylamide urea-denaturing gel and visualized via phosphorimager. Arrows indicate the positions of the oligonucleotide substrate (S) and the 3′ and 5′ cleavage products (3′P and 5′P, respectively). **(B)** Cycloheximide chase assay. Cells with the TAP tag fused to the C-terminus of Apn1 (genotypes indicated) were gown in YPD medium to log-phase, harvested, and adjusted to 2.5 OD_{600}. Cycloheximide was added to the growth medium and aliquots were removed from yeast cell cultures at the indicated timepoints. Cell lysates were resolved by SDS-PAGE and subjected to Western blot analysis by blotting with anti-TAP antibody. **(C)** Quantification of cycloheximide chase analysis results. Graph represents the average of at least four independent experiments. Error bars depict standard deviation. **(D)** Protein half-

life of wild type and Apn1 V156E variants. For each strain genotype, half-lives were estimated for each of four individual protein decay curves and then averaged as described in "materials and methods". Graph represents the decay curves based on average protein levels measured in four independent experiments for each data point for each strain. Intersection of dotted horizontal line and decay curves indicates half-life of the protein (50 on log scale). **(E)** Effects of proteosome inhibition on degradation of Apn1 variant proteins. Cells with the TAP tag fused to the C-terminus of Apn1 (genotypes indicated) were grown to log-phase in SD-complete media with proline as the nitrogen source and supplemented with 0.003% SDS. MG132 was added to the growth medium and after 30 minutes of growth at 30°C. Cycloheximide was then added to the cell culture and aliquots were removed at the indicated timepoints. Cell lysates were resolved by SDS-PAGE and subjected to Western blot analysis by blotting with anti-TAP antibody. Blots were reporobed with anti-Rpt5 antibody (Abcam) to visualize the relative levels of protein loaded. Blots were also probed with anti-ubiquitin P4D1 antibody (Upstate) to ensure MG132 could enter the cells and affect proteasome activity as indicated by increased levels of poly-ubiquitinated proteins.

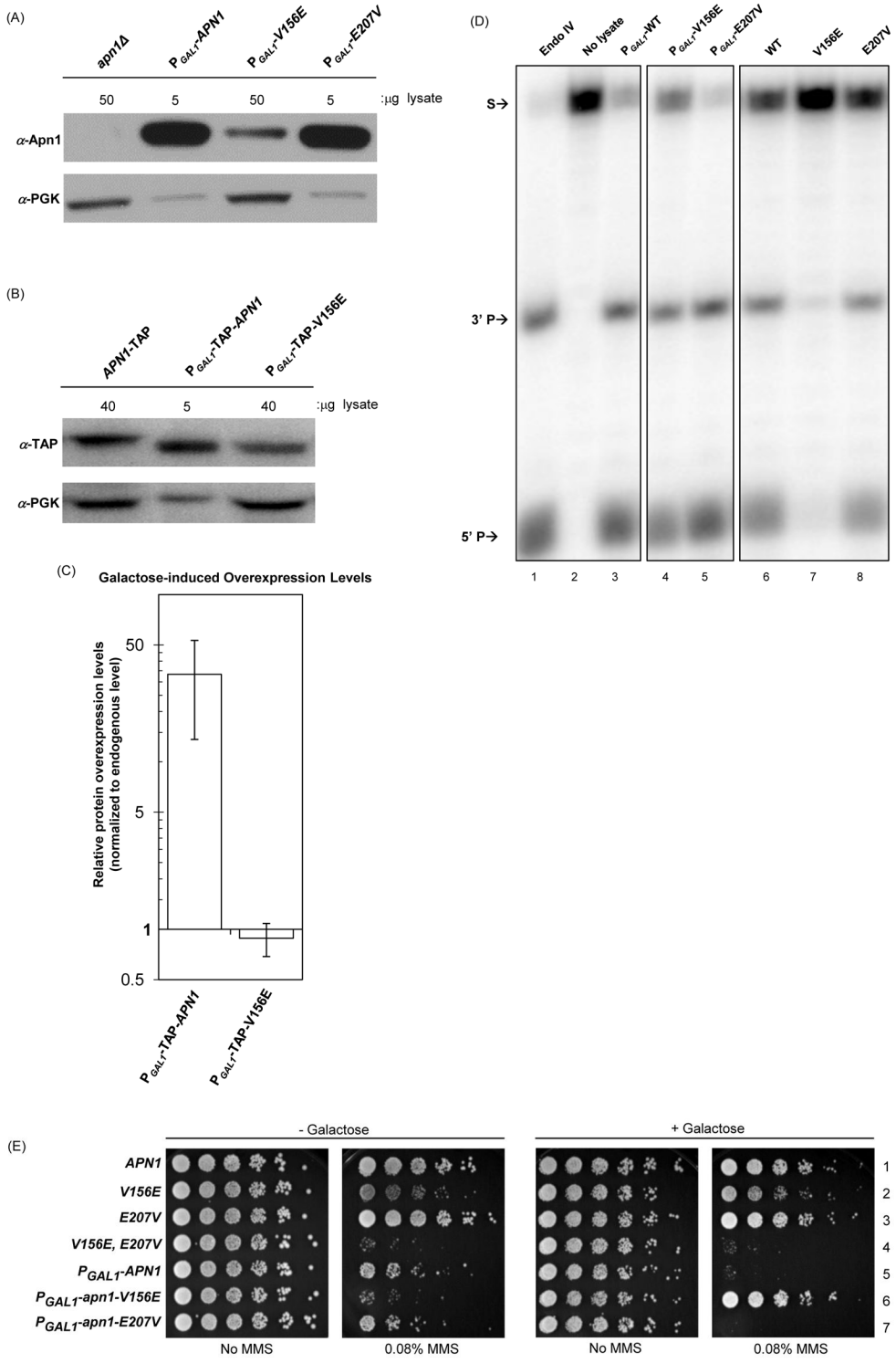

Figure 7. Apn1 V156E overexpression functionally restores cellular DNA repair activity

(A) Galactose-induced expression levels of Apn1 variant proteins. 5.0 μg aliquots of lysates from *P_{GAL1}-APN1* and *P_{GAL1}-apn1-E207V* cells and 50 μg aliquots of lysates from, *apn1ΔGAL-apn1-V156E* cells, grown in 2% galactose to induce *APN1* overexpression (except for the *apn1Δ* strain, which was used for negative control), were resolved by SDS-

PAGE and subjected to Western blot by probing with the anti-Apn1 antibody (top panel). Different amounts of lysates were used for comparison. Blots were reprobed with an antibody for PGK to determine the relative levels of protein loaded (bottom panel). **(B)** Galactose-induced expression levels of TAP-tagged Apn1 variant proteins. A 5.0 μg aliquot of lysate from P_{GAL1}-TAP-*APN1* and 40 μg aliquots of lysates from *APN1*-TAP and P_{GAL1}-TAP-apn1-V156E cells, grown in 2% galactose, were resolved by SDS-PAGE and subjected to Western blot by probing with the anti-TAP antibody (top panel). Blots were reprobed for PGK to determine the relative levels of protein loaded (bottom panel) **(D)** Quantification of protein levels relative to the levels of wild type protein expressed from the native promoter for three independent experiments. Error bars represent standard deviation. **(D)** AP incision activity in cells with galactose-induced overexpression of Apn1 variants. A THF site-containing oligonucleotide substrate labeled at both ends with ^{32}P was incubated with 0.5 μg of lysates from cells of the indicated strains grown in the presence of 2% galactose to induce *APN1* overexpression (lanes 3,4 and 5) or in YPD (lanes 6, 7 and 8) without induction. Note that the strains in lanes 6, 7, and 8 contained endogenous levels of Apn1 and Apn1 variants. Reaction products were resolved on a polyacrilamide urea-denaturing gel and visualized via phosphorimager. Arrows indicate the positions of the oligonucleotide substrate (S) and the 3′ and 5′ cleavage products (3′P and 5′P, respectively). Separate panels represent reactions resolved in non-adjacent lanes on the same gel. **(E)** MMS sensitivity of cells overexpressing Apn1 variants. 5-fold serial dilutions of cells were grown on YPD (denoted as "−Galactose") or 2% galactose (denoted as "+ Galactose") to induce *APN1* overexpression with or without 0.08% MMS. MMS sensitivity was assessed after incubation for two days at 30 °C. Strain genotypes with respect to *APN1* allele are indicated to the left of each row.

Table 1

Genotypes of strains used in this study

Strain	Relevant genotype or description	Reference/Source
hDNP16	*MATa/MATα rad1::kanMX/RAD1 ntg1::hphMX4/NTG1 ntg2::BSD/NTG2 apn1::TRP1/APN1 his7-1/his7-1 lys2Δ5′::LEU-lys2Δ3′/lys2Δ5′::LEU-lys2Δ3′ ade5-1/ade5-1 trp1-289/trp1-289 ura3-52/ura3-52*	[26]
hDNP19	*MATa/MATα rad1::kanMX/RAD1 ntg1::hphMX4/NTG1 ntg2::BSD/NTG2 apn1::TRP1/APN1 DSF1::URA3/DSF1 his7-1/his7-1 lys2Δ5′::LEU-lys2Δ3′/lys2Δ5′::LEU-lys2Δ3′ ade5-1/ade5-1 trp1-289/trp1-289 ura3-52/ura3-52*	[26]
DSC320[1]	*MATa [lys2::Alu-DIR-LEU2-lys2D5′] ade5-1 his7-2 leu2-3 112 trp1-289 ura3-52*	this study
DSC386[2]	*MATa [lys2::Alu-DIR-LEU2-lys2D5′] ade5-1 his7-2 leu2-3 112 trp1-289 ura3-52 ntg1::hyg ntg2::bsd*	this study
DSC393[2]	*MATa his7-1 lys2Δ5′::LEU-lys2Δ3′ ade5-1 trp1-289 ura3-52 apn1::TRP1 ntg1::hyg ntg2::bsd*	this study
DSC378[2]	*MATa his7-1 lys2Δ5′::LEU-lys2Δ3′ ade5-1 trp1-289 ura3-52 apn1::TRP1*	this study
DSC501	DSC0320 *apn1::KlURA3 kanMX4 GAL1*-I-*SceI*	this study
DSC502	DSC0386 *apn1::KlURA3 kanMX4 ntg1::hyg ntg2::bsd GAL1*-I-*SceI*	this study
YDM10[3]	*MATa [lys2::Alu-DIR-LEU2-lys2D5′] ade5-1 his7-2 leu2-3 112 trp1-289 ura3-52 apn1 V156E, E207V*	this study
DSC517[4]	DSC320 *apn1-V156E, E207V*	this study
DSC518[4]	DSC320 *apn1-V156E, E207V ntg1::hyg ntg2::bsd*	this study
DSC519[4]	DSC320 *apn1-V156E*	this study
DSC520[4]	DSC320 *apn1-E207V*	this study
DSC503	DSC320 *APN1-TRP1-TAP*	this study
DSC521	DSC320 *apn1-V156E, E207V TRP1 -TAP*	this study
DSC522	DSC320 *apn1-V156E TRP1-TAP*	this study
DSC523	DSC320 *apn1-E207V- TRP-TAP*	this study
DSC436	DSC320 *TRP1-*P_{GAL1}*-TAP-APN1*	this study
DSC519	DSC519 *TRP1-*P_{GAL1}-TAP-*apn1-V156E*	
DSC504	DSC320 *TRP1-*P_{GAL1}*-APN1*	this study
DSC525	DSC320 *TRP1-*P_{GAL1}*-apn1-V156E*	this study
DSC526	DSC320 *TRP1-*P_{GAL1}*-apn1-E207V*	this study

[1] This strain is a haploid spore of hDNP16.

[2] These strains are haploid spores of hDNP19.

[3] This strain was selected as MMS-sensitive after transformation of DSC502 with mutagenized *APN1* PCR fragments.

[4] In these strains, the mutations selected for in the *APN1* locus of YDM10 were re-introduced in order to confirm the MMS-sensitivity phenotype.